Available online at www.sciencedirect.com
SCIENCE DIRECT®
Journal of Solid State Chemistry 175 (2003) 197–206
JOURNAL OF SOLID STATE CHEMISTRY
http://elsevier.com/locate/jssc

The structural chemistry of $Bi_{14}MO_{24}$ (M = Cr, Mo, W) phases: bismuth oxides containing discrete MO_4 tetrahedra

T.E. Crumpton,[a] M.G. Francesconi,[b] and C. Greaves[a,*]

[a] School of Chemical Sciences, University of Birmingham, Edgbaston, Birmingham B15 2TT, UK
[b] Department of Chemistry, University of Hull, Hull HU6 7RX, UK

Received 25 February 2003; received in revised form 17 April 2003; accepted 25 April 2003

Abstract

The phases $Bi_{14}MO_{24}$ (M = Cr, Mo, W) have been studied using differential scanning calorimetry, variable temperature X-ray powder diffraction and neutron powder diffraction. All three compounds were found to undergo a phase change, on cooling, from the previously reported tetragonal symmetry ($I4/m$) to monoclinic symmetry ($C2/m$). Transition temperatures were determined to be ~306 K (M = W) and ~295 K (M = Mo), whereas a gradual transition between 275 and 200 K was observed for M = Cr. The high and low temperature structures are very similar, as indicated by the relationship between the monoclinic and tetragonal unit cell parameters: $a_m = \sqrt{2}a_t$, $b_m = c_t$, $c_m = a_t$, $\beta \sim 135°$. High-resolution neutron powder diffraction data, collected at 400 and 4 K, were used to establish the nature of the transition, which was found to involve a reduction in the statistical possibilities for orientation of the MO_4 tetrahedra. However, in both tetragonal and monoclinic variants, a degree of orientational disorder of the tetrahedra occurs to give partially occupied sites in the average unit cell.

Keywords: Bismuth oxide; Bismuth chromium oxide, structure; Bismuth molybdenum oxide, structure; Bismuth tungsten oxide, structure

1. Introduction

There has been much interest in δ-Bi_2O_3 owing to its excellent oxide ion conduction properties, the conductivity being ~1 S cm^{-1} at 1023 K [1]. However, δ-Bi_2O_3 is stable only between 937 K and the melting point of Bi_2O_3 at 1097 K. Two metastable Bi_2O_3 phases can form on cooling: the tetragonal β-phase at 923 K and the body-centered cubic γ-phase at 912 K. At lower temperatures, the room temperature stable monoclinic α-phase forms [2].

Substitution of Bi using small amounts of tetrahedral ions is known to stabilize the γ-Bi_2O_3 structure. Sillén [3] identified $Bi_{12}SiO_{20}$, and Harwig [4] indicated that $Bi_{12}GeO_{20}$ is isomorphous with γ-Bi_2O_3; there are more than 40 of such sillenite phases known [5]. δ-Bi_2O_3 has been reported to have an oxygen deficient fluorite structure [4,6] in which structural disorder in the O sublattice is responsible for the high oxide ion conductivity of this phase. Although the basic structure can be stabilized at room temperature by doping with isovalent (e.g., Y^{3+}), or aliovalent (e.g., Ta^{5+}) cations, the Arrhenius energy for oxygen migration is increased, which results in much lower conductivities [1]: e.g., 30% Y_2O_3/Bi_2O_3 has an Arrhenius energy of ~0.7 eV compared with a value of ~0.4 eV for pure δ-Bi_2O_3.

Using a solid state reaction between α-Bi_2O_3 and $(NH_4)_2SO_4$, in the mole ratio of 14:1 (Bi:SO_4), Francesconi et al. [7] formed the new phase $Bi_{14}SO_{24}$. The body-centered tetragonal ($I4/m$) structure is a superstructure of the cubic fluorite subcell of δ-Bi_2O_3, with SO_4^{2-} anions occupying the origin and body center of the enlarged unit cell [7]. A schematic representation of the Bi/S sublattice is shown in Fig. 1 and highlights the relationship of the body-centered tetragonal supercell (a = 8.7 Å, c = 17.3 Å) to the cubic δ-Bi_2O_3 subcell (a ~ 5.7 Å).

Neutron powder diffraction (NPD) studies have been performed on $Bi_{14}WO_{24}$ and $Bi_{14}MoO_{24}$ [8], and also on $Bi_{14}CrO_{24}$ [9]. All were reported to have body-centered tetragonal, $I4/m$, structures which are closely related to that previously reported for $Bi_{14}SO_{24}$ [7]: MO_4^{2-} oxoanions (M = W, Mo, or Cr), occupy the origin and body center of the unit cell.

*Corresponding author. Fax: +44-121-414-4442.
E-mail address: c.greaves@bham.ac.uk (C. Greaves).

0022-4596/03/$ - see front matter © 2003 Elsevier Inc. All rights reserved.
doi:10.1016/S0022-4596(03)00246-9

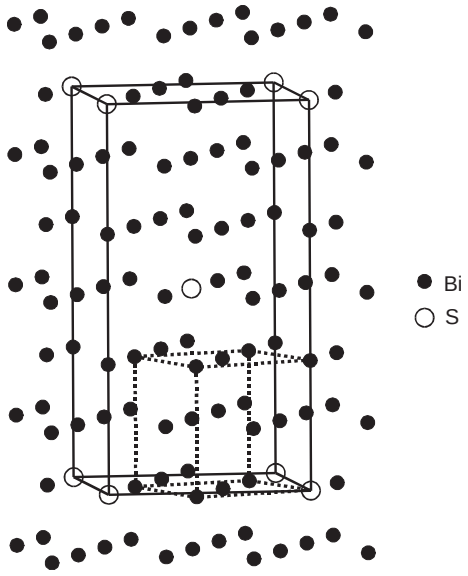

Fig. 1. The body-centered tetragonal supercell of $Bi_{14}SO_{24}$ and its relationship to the face-centered cubic δ-Bi_2O_3 subcell (broken lines).

The proposed tetragonal models indicate significant disorder of the O atoms coordinating M. For $Bi_{14}SO_{24}$, Francesconi et al. [7] proposed that the tetrahedral coordination around S was best approximated by a model containing two of the coordinating O atoms in the same xy plane as S with an O–S–O angle of 90°; two apical O atoms were positioned above and below the S xy plane. Ling et al. [8] proposed a slightly different model for both $Bi_{14}WO_{24}$, and $Bi_{14}MoO_{24}$: octahedral coordination of the W or Mo by the O atoms, but with each WO_6 octahedron having one axial and one equatorial O site vacant. Warda et al. [9] proposed a similar CrO_4 orientation in $Bi_{14}CrO_{24}$, with one O atom aligned on the z (C_4) axis and the other three O atoms being displaced below the Cr xy plane.

At room temperature, a degree of orientational disorder therefore occurs for the tetrahedral MO_4 oxoanions in each of the phases $Bi_{14}MO_{24}$ (M = Cr, Mo, W). The possibility of ordering these groups has been investigated by performing a variable temperature NPD structural investigation of all three phases. In this paper we report that new monoclinic ($C2/m$) structures can be produced for all three materials. For M = Mo and W, the transition temperature was found to be close to ambient temperature, but for M = Cr, a significantly lower temperature was required to induce the transition.

2. Experimental

$Bi_{14}WO_{24}$, $Bi_{14}MoO_{24}$ and $Bi_{14}CrO_{24}$ were synthesized from intimate mixtures of high purity Bi_2O_3 with either WO_3, MoO_3, or Cr_2O_3, in stoichiometric amounts; the mixtures were then heated to 1023 K for 12 h. Several subsequent cycles of regrinding and reheating were used to ensure complete reaction to give single phase products. Chemical analysis (ICP emission spectroscopy) confirmed that no detectable bismuth loss occurred during synthesis.

The effect of cooling rate on the basic structure of these phases was investigated. Samples were either quenched from 1023 K to room temperature, by removal from the furnace and immediately tipping the powder into a cold alumina boat, or cooled slowly using programmed cooling at $-20\,K\,h^{-1}$. X-ray powder diffraction, XPD, (Siemens D5000, primary beam monochromator, transmission mode, with position sensitive detector), was used for phase characterization and basic structure examination. DSC data were obtained from heating and cooling cycles, (Perkin Elmer, Pyris 1 calorimeter), and variable temperature XPD data were collected using a Bruker AXS D5005 diffractometer.

Time-of-flight NPD data, using a cryofurnace, were collected at 4 and 400 K, with the high-resolution powder diffractometer HRPD at the Rutherford Appleton Laboratory. Structure refinement was achieved using the General Structure Analysis System (GSAS) [10] refinement program.

3. Results and discussion

XPD data showed that the quenched samples of $Bi_{14}WO_{24}$ and $Bi_{14}MoO_{24}$ consisted predominately of the tetragonal phase, previously reported [8]. However, for slow cooled samples, extensive line splitting was apparent in the XPD patterns and indicated a new phase with lower symmetry; the splittings were consistent with monoclinic, $C2/m$, symmetry. $Bi_{14}CrO_{24}$, on the other hand, formed only the tetragonal phase with no evidence of a transition above 290 K.

DSC data revealed that on heating, slow cooled samples of both $Bi_{14}WO_{24}$ and $Bi_{14}MoO_{24}$ underwent endothermic transitions with peak onset temperatures of 306 and 295 K, respectively (Figs. 2 and 3). As seen in these figures, more ill-defined exothermic peaks, with similar onset temperatures, were observed on cooling. No evidence for a similar transition was found for $Bi_{14}CrO_{24}$ within the accessible temperature range, 133–343 K.

To confirm that the phase change revealed by DSC corresponded to the tetragonal–monoclinic structural transition, variable temperature XPD data were collected. XPD patterns were recorded at several temperatures in the vicinity of the transition temperature indicated by DSC. Many of the higher angle peaks of the tetragonal phase were split at temperatures below the transition temperature, Fig. 4, indicating that the thermodynamic transition corresponds to the structural

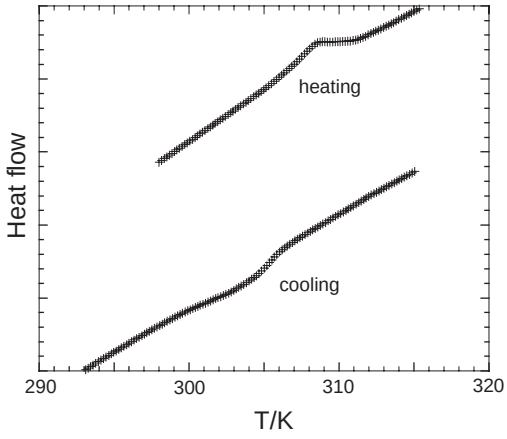

Fig. 2. Heating and cooling DSC curves for $Bi_{14}WO_{24}$.

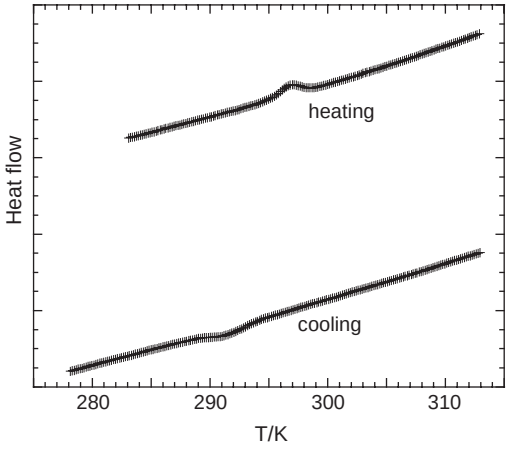

Fig. 3. Heating and cooling DSC curves for $Bi_{14}MoO_{24}$.

phase change from tetragonal symmetry (high temperature), to monoclinic (low temperature).

Although the DSC investigation of $Bi_{14}CrO_{24}$, provided no evidence for a structural transition, variable temperature XPD investigations produced split high angle peaks, which were slowly formed over a range of temperature between 275 and 200 K. At 275 K, the pattern was consistent with the tetragonal phase. Some evidence of slight peak splitting occurred at 250 K, and at 200 K the peak splitting was complete as the monoclinic phase formed, (Fig. 5). $Bi_{14}CrO_{24}$ therefore also undergoes a low temperature transition to a monoclinic form, but the transition is so broad that it was undetectable by DSC.

Fig. 6 shows the relationship between the body-centered tetragonal supercell (Fig. 6(a)) and the monoclinic structure (Fig. 6(b)): $a_m = a_t\sqrt{2}$, $c_m = a_t$, $b_m = c_t$. The MO_4^{2-} groups describe body-centered and C-centered lattices in the tetragonal and monoclinic phases. The β angle is just a fraction of a degree less

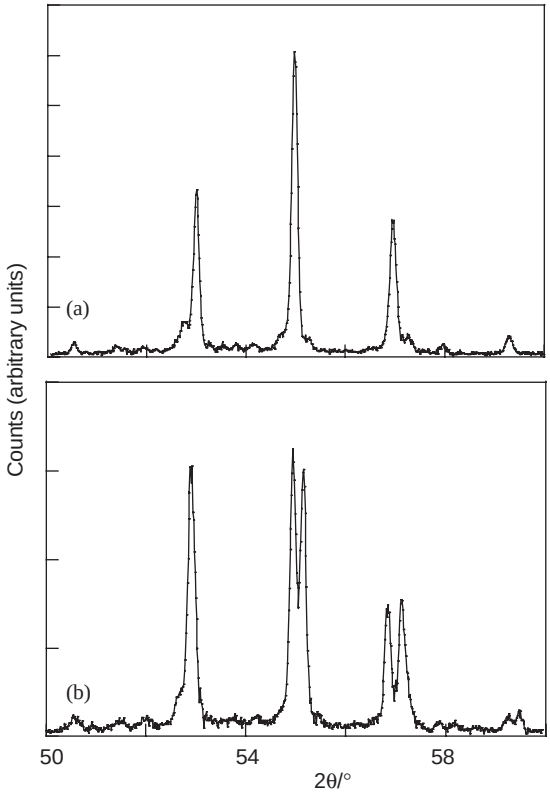

Fig. 4. X-ray powder diffraction patterns from $Bi_{14}MoO_{24}$ at (a) 305 K and (b) 270 K showing split peaks consistent with monoclinic symmetry.

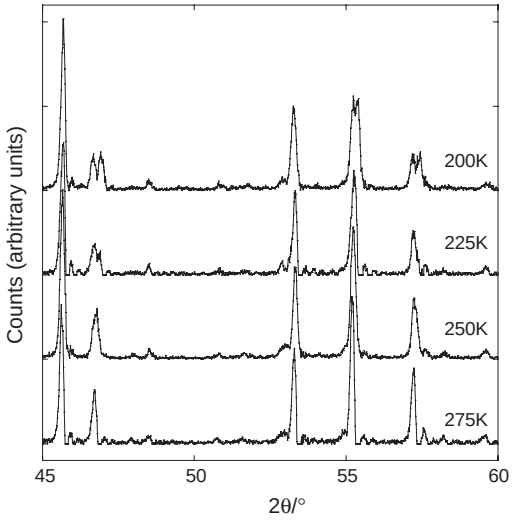

Fig. 5. X-ray powder diffraction data from $Bi_{14}CrO_{24}$ at 200–275 K.

than the ideal 135° angle of the tetragonal structure. Because of this slight, but significant, change in symmetry, NPD data were collected using the very high-resolution diffractometer, HRPD.

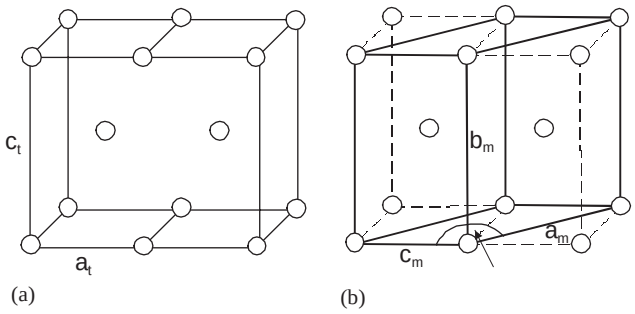

Fig. 6. The relationship between the tetragonal and monoclinic unit cells: (a) 2 adjacent body-centered tetragonal cells; (b) the C-centered monoclinic cell. The subscripts '*t*' and '*m*' refer to tetragonal and monoclinic axes, respectively.

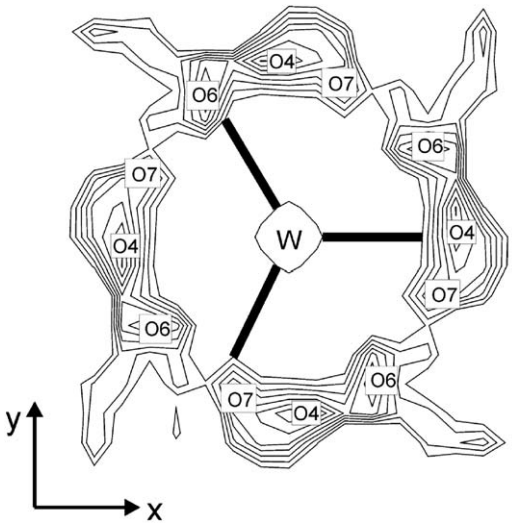

Fig. 7. Difference Fourier map of the region around the WO_4^{2-} anion in $Bi_{14}WO_{24}$ at 400 K. The presence of several equivalent positions results from the 4-fold axis.

Refinement of the tetragonal structures was based on the 400 K data sets, and the initial model was derived from $Bi_{14}SO_{24}$ [7], space group $I4/m$, although the O atoms in the tetrahedral MO_4 groups were excluded. As previously suggested for the M=Cr phase [9], it was found that all M atoms were displaced from the origin along the [001] axis. In accordance with the mirror plane perpendicular to z, the M site was therefore split into two half occupied sites, which resulted in considerable lowering of the isotropic temperature factor for M, and an improved fit. The O atoms bonded to M were then sought using Difference Fourier techniques. From locations indicated by the Fourier maps, and refinement of site occupancies, it became clear that each MO_4 group had one O atom (O5) directed along +[001] or −[001], with the three remaining O atoms (O4, O6 and O7) being approximately coplanar (similar z/c parameters) and located on the opposite side of M. Because of the $4/m$ origin symmetry, for tetrahedral MO_4, the O4, O6, and O7 site occupancies are only 0.125, and the Fourier maps (see Fig. 7) appear quite complex. In all cases, inclusion of the O atoms of the MO_4 groups into the refinements produced significant lowering of the R factor values. The refined atomic parameters for the tetragonal phases are given in Tables 1–3. In all cases it can be seen that the thermal parameters for the MO_4 O atoms are quite high, which probably relate to oscillations of the groups around the central M atom.

Selected O–M–O bond angles for the MO_4^{2-} anions are given in Tables 4–6, and are in good agreement with the expected 109.5° for regular tetrahedral coordination. The structural data reported here are considered to be the most reliable for the high temperature tetragonal structures of $Bi_{14}CrO_{24}$, $Bi_{14}MoO_{24}$ and $Bi_{14}WO_{24}$. It is clear that a statistical distribution of the orientation of the MO_4 groups is required for compatibility with the high symmetry $I4/m$ space group. It was anticipated that the structural transition observed on cooling would correspond to a reduction in the number of possible orientational configurations. However, elimination of one of the two equivalent orientations of M–O5 along +[001] or −[001] would require 180° rotation, which may not be possible at the low temperatures involved.

The approximate atomic positions in the monoclinic, $C2/m$, cell were calculated from the tetragonal structure to provide the initial model for structure refinement, after eliminating the O atoms of the MO_4 groups. As with the tetragonal refinements, the M atoms were found to be displaced off the ideal site at the origin, along the [010] axis, and a split site with fractional site occupancy of 0.5 was again used.

The four O atoms coordinated to M were then located using Difference Fourier methods. Strong intensity was found for two O atoms on the xz plane of M (Fig. 8). These two O atoms were assigned O8, and O9. The position of atom O10 was then located just below the xz plane containing M, and after inclusion of these atoms, atom O7 was found above the xz plane of M close to the [010] axis; the MO_4 groups are therefore arranged similarly to that found for the tetragonal structure. The MO_4^{2-} oxoanion is located on the 2-fold axis and the mirror plane of the $C2/m$ space group and this necessarily creates orientational disorder, as indicated in Fig. 8. The refined atomic parameters are given in Tables 7–9. The temperature factors were considered to be reasonable, and significantly lower than those observed for the tetragonal, 400 K data. Selected bond distances and angles are given in Tables 10–12, and support the tetrahedral coordination around M. The final refined observed, calculated, and difference powder neutron diffraction profiles, for the tetragonal, and monoclinic phase of $Bi_{14}CrO_{24}$, are given in Figs. 9 and 10, and are also representative of data obtained for the Mo and W analogues.

Table 1
Refined atomic parameters (NPD) for $Bi_{14}WO_{24}$ in space group $I4/m$ at 400 K

Atom	Position	x	y	z	$U_i/U_e * 100$ Å^2	Occupancy
W	4*e*	0.0000	0.0000	0.0150(8)	1.5(4)	2
Bi1	8*h*	0.2136(3)	0.4420(3)	0.0000	1.73(7)	8
Bi2	16*i*	0.3002(3)	0.1066(3)	0.1704(1)	1.60(4)	16
Bi3	4*e*	0.5000	0.5000	0.1565(3)	2.5(1)	4
O1	8*g*	0.5000	0.0000	0.1237(4)	3.1(1)	8
O2	16*i*	0.0733(3)	0.2555(4)	0.2573(2)	2.21(7)	16
O3	16*i*	0.3228(3)	0.6234(4)	0.0776(2)	2.22(7)	16
O4	16*i*	0.023(3)	0.197(2)	0.0183(9)	5.1(6)	2
O5	4*e*	0.0000	0.0000	0.1155(9)	4.0(3)	2
O6	16*i*	0.132(2)	0.132(2)	0.022(1)	3.8(8)	2
O7	16*i*	0.980(1)	0.197(2)	0.018(1)	5.1(6)	2

$I4/m$; $a = b = 8.7296(1)$, $c = 17.3613(2)$; $R_{wp} = 0.033$, $R_{exp} = 0.017$.

Table 2
Refined atomic parameters (NPD) for $Bi_{14}MoO_{24}$ in space group $I4/m$ at 400 K

Atom	Position	x	y	z	$U_i/U_e * 100$ Å^2	Occupancy
Mo	4*e*	0.0000	0.0000	0.0145(5)	2.7(2)	2
Bi1	8*h*	0.2130(2)	0.4409(2)	0.0000	2.07(5)	8
Bi2	16*i*	0.3001(2)	0.1062(2)	0.17017(9)	1.91(3)	16
Bi3	4*e*	0.5000	0.5000	0.1571(2)	2.62(8)	4
O1	8*g*	0.5000	0.0000	0.1229(3)	3.45(7)	8
O2	16*i*	0.0738(2)	0.2547(3)	0.2567(1)	2.53(5)	16
O3	16*i*	0.3223(2)	0.6239(3)	0.0776(1)	2.40(5)	16
O4	16*i*	0.029(1)	0.193(1)	0.0282(9)	5.7(4)	2
O5	4*e*	0.0000	0.0000	0.1161(5)	3.5(2)	2
O6	16*i*	0.131(2)	0.124(2)	0.022(1)	4.3(6)	2
O7	16*i*	0.980(1)	0.206(1)	0.0090(9)	5.2(4)	2

$I4/m$; $a = b = 8.7232(1)$, $c = 17.3446(1)$; $R_{wp} = 0.029$, $R_{exp} = 0.020$.

Table 3
Refined atomic parameters (NPD) for $Bi_{14}CrO_{24}$ in space group $I4/m$ at 400 K

Atom	Position	x	y	z	$U_i/U_e * 100$ Å^2	Occupancy
Cr	4*e*	0.0000	0.0000	0.0159(9)	2.1(4)	2
Bi1	8*h*	0.2125(3)	0.4374(2)	0.0000	1.31(6)	8
Bi2	16*i*	0.2989(2)	0.1065(2)	0.16924(9)	1.23(3)	16
Bi3	4*e*	0.5000	0.5000	0.1578(2)	1.93(9)	4
O1	8*g*	0.5000	0.0000	0.1230(3)	2.50(7)	8
O2	16*i*	0.0752(3)	0.2527(3)	0.2571(1)	1.96(5)	16
O3	16*i*	0.3187(3)	0.6229(3)	0.0778(2)	1.83(5)	16
O4	16*i*	0.012(3)	0.200(2)	0.016(1)	2.2(9)	2
O5	4*e*	0.0000	0.0000	0.1108(7)	4.8(3)	2
O6	16*i*	0.109(4)	0.132(4)	0.020(1)	5.1(8)	2
O7	16*i*	0.955(6)	0.179(5)	0.018(2)	6.2(1)	2

$I4/m$; $a = b = 8.6402(1)$, $c = 17.1599(2)$; $R_{wp} = 0.034$, $R_{exp} = 0.025$.

Refinements using the lower symmetry space group Cm resulted in similar Difference Fourier maps to that shown in Fig. 8, indicating the presence of the 2-fold axis, and supporting the $C2/m$ space group. The general structure of the monoclinic phase, viewed along [101], is shown in Fig. 11; just one of the possible orientations of the MO_4 groups is depicted.

Comparison of the orientation of the MO_4 units reveals that little change occurs at the tetragonal–monoclinic phase change. The atom O5 lies on the *c*-axis

Table 4
Selected bond distances (Å) and angles (deg) for $Bi_{14}WO_{24}$ in space group $I4/m$ at 400 K

W–O4	1.73(1)	O1–Bi2–O2	92.8(2)
W–O5	1.75(2)		95.4(2)
W–O6	1.76(3)		
W–O7	1.73(1)	O1–Bi2–O3	82.5(1)
O4–W–O5	108.5(6)	O2–B2–O2	95.4(1)
		O2–Bi2–O3	79.3(2)
			174.1(2)
O4–W–O6	115.3(8)		
O4–W–O7	102.5(1)	Bi1–O3	2.288(4)[× 2]
O5–W–O6	111.8(9)		2.219(4)[× 2]
O5–W–O7	108.5(1)		
O6–W–O7	115.9(2)	O3–Bi1–O3	72.2(2)
			72.5(2)[× 2]
			74.8(2)
Bi2–O1	2.138(3)		114.0(2)[× 2]
Bi2–O3	2.570(4)		
Bi2–O2	2.060(4)	Bi3–O3	2.330(5)[× 4]
Bi2–O2	2.212(4)		
		O3–Bi3–O3	69.8(1)[× 4]
			108.0(3)[× 2]

Table 5
Selected bond distances (Å) and angles (deg) for $Bi_{14}MoO_{24}$ in space group $I4/m$ at 400 K

Mo–O4	1.72(1)	O1–Bi2–O2	93.2(1)
Mo–O5	1.76(1)		95.7(1)
Mo–O6	1.70(2)		
Mo–O7	1.81(1)	O1–Bi2–O3	82.39(9)
		O2–B2–O2	95.5(9)
		O2–Bi2–O3	79.4(1)
O4–Mo–O5	113.5(5)		174.4(1)
O4–Mo–O6	112(6)		
O4–Mo–O7	105.3(2)	Bi1–O3	2.295(3)[× 2]
O5–Mo–O6	111.9(6)		2.215(3)[× 2]
O5–Mo–O7	102.7(9)		
O6–Mo–O7	118.4(4)	O3–Bi1–O3	71.8(1)
			72.7(1)[× 2]
			74.8(1)
Bi2–O1	2.138(3)		114.5(1)[× 2]
Bi2–O3	2.563(3)		
Bi2–O2	2.209(3)	Bi3–O3	2.340(3)[× 4]
Bi2–O2	2.071(3)		
		O3–Bi3–O3	69.67(9)[× 4]
			107.8(2)[× 2]

Table 6
Selected bond distances (Å) and angles (deg) for $Bi_{14}CrO_{24}$ in space group $I4/m$ at 400 K

Cr–O4	1.73(2)	O1–Bi2–O2	95.4(2)
Cr–O5	1.63(2)		93.0(1)
Cr–O6	1.60(2)		
Cr–O7	1.60(3)	O1–Bi2–O3	82.1(1)
		O2–B2–O2	95.5(2)
		O2–Bi2–O3	79.1(2)
O4–Cr–O5	108.6(8)		173.8(1)
O4–Cr–O6	114(1)		
O4–Cr–O7	107(2)	Bi1–O3	2.280(4)[× 2]
O5–Cr–O6	113(1)		2.204(4)[× 2]
O5–Cr–O7	110(2)		
O6–Cr–O7	113(2)	O3–Bi1–O3	71.7(2)
			73.3(2)[× 2]
			74.6(2)
Bi2–O1	2.120(4)		115.0(2)[× 2]
Bi2–O3	2.506(4)		
Bi2–O2	2.064(4)	Bi3–O3	2.338(5)[× 4]
Bi2–O2	2.213(4)		
		O3–Bi3–O3	69.8(1)[× 4]
			108.1(2)[× 2]

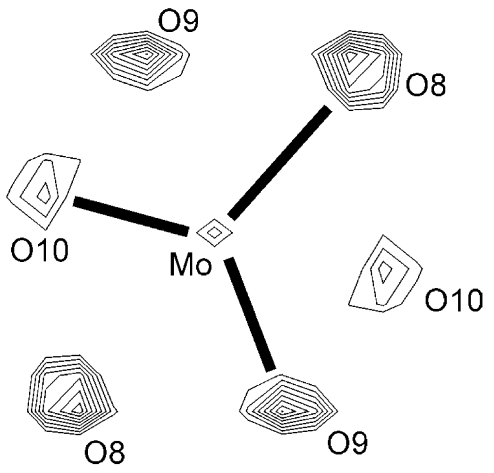

Fig. 8. Difference Fourier map of the region around the MoO_4^{2-} anion in $Bi_{14}MoO_{24}$ at 4 K. Orientational disorder results from the 2-fold axis.

($I4/m$) and transforms to O7 which is very close to the derived *b*-axis ($C2/m$); on the opposite side of *M* lies a triangle of O atoms: O4, O6, O7 ($I4/m$) and O8, O9, O10 ($C2/m$). The principal change involves the reduction in the number of equivalent positions for the triangular arrangement, from four in the tetragonal structure to two in the low temperature modification. In other words, on cooling, the four equivalent locations for O4 (for example) reduce to two as the small structural distortion reduces the C4 symmetry axis to C2.

Bond valence sum calculations [11] revealed that the bond lengths are consistent with *M*(VI). The *M*–O bond lengths (Tables 4–6) for WO_4^{2-}, MoO_4^{2-}, and CrO_4^{2-} in the tetragonal form produced values of 6.42, 6.20, and 6.13, respectively. For the monoclinic phase, the corresponding data in Tables 10–12 produced values of 6.27, 6.14, and 5.65.

The slight distortion of the tetragonal phase to give the monoclinic structure, transforms the three Bi sites into five: Bi1 ($I4/m$) becomes Bi1 and Bi2 ($C2/m$); Bi2 ($I4/m$) becomes Bi3 and Bi4 ($C2/m$); Bi3 ($I4/m$) becomes Bi5 ($C2/m$). In the tetragonal phase, Bi1 and Bi3 form BiO_4e square pyramids (where e represents a

Table 7
Refined atomic parameters (NPD) for $Bi_{14}WO_{24}$ in space group $C2/m$ at 4 K

Atom	Position	x	y	z	$U_i/U_e * 100$ Å^2	Occupancy
W	4*g*	0.0000	0.0183(7)	0.0000	0.7(2)	2
Bi1	4*i*	0.4432(5)	0.000	0.6572(7)	0.6(1)	4
Bi2	4*i*	0.7874(6)	0.000	0.2262(9)	0.5(1)	4
Bi3	8*j*	0.1060(5)	0.1691(2)	0.4058(6)	0.41(8)	8
Bi4	8*j*	0.7000(5)	0.1698(2)	0.8046(7)	0.73(8)	8
Bi5	4*h*	0.5000	0.1588(3)	0.0000	1.4(1)	4
O1	4*h*	0.0000	0.1237(5)	0.5000	1.0(2)	4
O2	4*g*	0.5000	0.1235(4)	0.5000	0.4(1)	4
O3	8*j*	0.2541(6)	0.2600(3)	0.3282(8)	0.7(1)	8
O4	8*j*	0.9266(5)	0.2588(3)	0.1781(7)	0.9(1)	8
O5	8*j*	0.6243(6)	0.0772(3)	0.9483(8)	1.1(1)	8
O6	8*j*	0.6775(7)	0.0757(3)	0.304(1)	2.0(2)	8
O7	8*j*	0.981(4)	0.1203(9)	0.995(5)	0.8(5)	2
O8	4*i*	0.210(2)	0.0000	0.220(2)	0.9(2)	2
O9	4*i*	0.934(2)	0.0000	0.754(2)	0.06(2)	2
O10	8*j*	0.916(3)	0.023(1)	0.073(4)	2.3(5)	2

$C2/m$; $a = 12.2100(1)$, $b = 17.3652(2)$, $c = 8.6460(1)$, $\beta = 134.4805(2)$; $R_{wp} = 0.052$, $R_{exp} = 0.012$.

Table 8
Refined atomic parameters (NPD) for $Bi_{14}MoO_{24}$ in space group $C2/m$ at 4 K

Atom	Position	x	y	z	$U_i/U_e * 100$ Å^2	Occupancy
Mo	4*g*	0.0000	0.0178(5)	0.0000	0.2(3)	2
Bi1	4*i*	0.4428(5)	0.0000	0.6563(7)	1.2(1)	4
Bi2	4*i*	0.7885(6)	0.0000	0.2275(9)	1.1(1)	4
Bi3	8*j*	0.1064(5)	0.1686(2)	0.4061(6)	0.73(3)	8
Bi4	8*j*	0.6996(5)	0.1700(2)	0.8050(7)	0.96(8)	8
Bi5	4*h*	0.5000	0.1597(3)	0.0000	1.5(1)	4
O1	4*h*	0.0000	0.1233(5)	0.5000	1.7(1)	4
O2	4*g*	0.5000	0.1223(4)	0.5000	0.7(1)	4
O3	8*j*	0.2542(5)	0.2582(3)	0.3288(8)	0.9(1)	8
O4	8*j*	0.9257(5)	0.2597(3)	0.1763(7)	0.7(1)	8
O5	8*j*	0.6230(6)	0.0768(3)	0.9458(8)	1.2(1)	8
O6	8*j*	0.6782(7)	0.0767(4)	0.304(1)	2.1(2)	8
O7	8*j*	0.993(9)	0.1225(9)	0.004(1)	2.0(5)	2
O8	4*i*	0.206(2)	0.0000	0.216(3)	2.7(4)	2
O9	4*i*	0.929(2)	0.0000	0.748(3)	1.0(3)	2
O10	8*j*	0.918(3)	0.025(1)	0.073(4)	2.1(5)	2

$C2/m$; $a = 12.2110(2)$, $b = 17.3356(2)$, $c = 8.6454(1)$, $\beta = 134.5138(3)$; $R_{wp} = 0.049$, $R_{exp} = 0.011$.

Table 9
Refined atomic parameters (NPD) for $Bi_{14}CrO_{24}$ in space group $C2/m$ at 4 K

Atom	Position	x	y	z	$U_i/U_e * 100$ Å^2	Occupancy
Cr	4*g*	0.0000	0.0205(8)	0.0000	0.6(2)	2
Bi1	4*i*	0.4380(4)	0.0000	0.6502(6)	0.21(9)	4
Bi2	4*i*	0.7893(5)	0.0000	0.2236(7)	0.7(1)	4
Bi3	8*j*	0.1066(4)	0.1680(2)	0.4047(5)	0.55(7)	8
Bi4	8*j*	0.7015(4)	0.1692(2)	0.8070(6)	0.39(7)	8
Bi5	4*h*	0.5000	0.1592(3)	0.0000	1.1(1)	4
O1	4*h*	0.0000	0.1217(5)	0.5000	1.2(1)	4
O2	4*g*	0.5000	0.1231(4)	0.5000	0.8(1)	4
O3	8*j*	0.2539(5)	0.2593(3)	0.3293(6)	0.6(1)	8
O4	8*j*	0.9231(4)	0.2572(3)	0.1744(7)	1.0(1)	8
O5	8*j*	0.6233(5)	0.0771(3)	0.9422(7)	0.9(1)	8
O6	8*j*	0.6808(6)	0.0775(3)	0.3036(8)	1.5(1)	8
O7	8*j*	0.011(3)	0.1177(7)	0.029(4)	0.6(4)	2
O8	4*i*	0.198(1)	0.0000	0.203(2)	0.8(2)	2
O9	4*i*	0.938(1)	0.0000	0.767(2)	0.8(2)	2
O10	8*j*	0.905(2)	0.0198(7)	0.049(2)	0.4(4)	2

$C2/m$; $a = 12.1697(1)$, $b = 17.1842(2)$, $c = 8.6176(1)$, $\beta = 134.6719(1)$; $R_{wp} = 0.044$, $R_{exp} = 0.022$.

Table 10
Selected bond distances (Å) and angles (deg) for $Bi_{14}WO_{24}$ in space group $C2/m$ at 4 K

W–O7	1.78(2)	O7–W–O8	105(1)	Bi3–O1	2.107(5)	O1–Bi3–O3	92.6(2)
W–O8	1.86(1)	O7–W–O9	103(1)	Bi3–O3	2.054(7)	O1–Bi3–O4	96.4(2)
W–O9	1.69(1)	O7–W–O10	109(1)	Bi3–O4	2.250(6)	O1–Bi3–O6	82.9(2)
W–O10	1.70(2)	O8–W–O9	111.0(7)	Bi3–O6	2.573(8)	O3–Bi3–O4	95.8(3)
		O8–W–O10	108(1)			O3–Bi3–O6	78.8(2)
		O9–W–O10	120(1)			O4–Bi3–O6	174.5(3)
				Bi4–O2	2.129(5)	O2–Bi4–O3	96.4(2)
				Bi4–O3	2.234(7)	O2–BI4–O4	92.8(2)
Bi1–O5	2.285(6)[× 2]	O5–Bi1–O5	71.8(3)	Bi4–O4	2.066(7)	O2–Bi4–O5	82.7(2)
Bi1–O6	2.169(7)[× 2]	O5–Bi1–O6	115.0(3)	Bi4–O5	2.567(7)	O3–Bi4–O4	94.9(3)
		O6–Bi1–O6	74.6(4)			O3–Bi4–O5	173.3(3)
Bi2–O5	2.198(7)[× 2]	O5–Bi2–O5	75.2(3)			O4–Bi4–O5	78.5(2)
Bi2–O6	2.291(7)[× 2]	O5–Bi2–O6	113.7(3)	Bi5–O5	2.337(7)[× 2]	O5–Bi5–O5	105.3(4)
		O6–Bi2–O6	70.0(3)	Bi5–O6	2.389(7)[× 2]	O5–Bi5–O6	68.5(2)
						O6–Bi5–O6	105.6(4)

Table 11
Selected bond distances (Å) and angles (deg) for $Bi_{14}MoO_{24}$ in space group $C2/m$ at 4 K

Mo–O7	1.82(2)	O7–Mo–O8	101(3)	Bi3–O1	2.107(5)	O1–Bi3–O3	93.0(2)
Mo–O8	1.82(2)	O7–Mo–O9	102(2)	Bi3–O3	2.071(7)	O1–Bi3–O4	96.5(2)
Mo–O9	1.71(2)	O7–Mo–O10	113(2)	Bi3–O4	2.271(6)	O1–Bi3–O6	83.0(2)
Mo–O10	1.67(2)	O8–Mo–O9	112.6(8)	Bi3–O6	2.548(8)	O3–Bi3–O4	94.8(3)
		O8–Mo–O10	106(1)			O3–Bi3–O6	79.2(2)
		O9–Mo–O10	120(1)			O4–Bi3–O6	174.1(3)
				Bi4–O2	2.136(5)	O2–Bi4–O3	96.4(2)
				Bi4–O3	2.216(7)	O2–Bi4–O4	93.4(2)
Bi1–O5	2.272(6)[× 2]	O5–Bi1–O5	71.7(3)	Bi4–O4	2.051(7)	O2–Bi4–O5	82.1(2)
Bi1–O6	2.190(7)[× 2]	O5–Bi1–O6	115.0(3)	Bi4–O5	2.561(7)	O3–Bi4–O4	96.0(3)
		O6–Bi1–O6	75.0(4)			O3–Bi4–O5	174.1(3)
Bi2–O5	2.209(7)[× 2]	O5–Bi2–O5	74.1(3)			O4–Bi4–O5	78.3(2)
Bi2–O6	2.293(7)[× 2]	O5–Bi2–O6	113.6(3)	Bi5–O5	2.352(7)[× 2]	O5–Bi5–O5	104.5(4)
		O6–Bi2–O6	71.1(3)	Bi5–O6	2.385(7)[× 2]	O5–Bi5–O6	68.2(2)
						O6–Bi5–O6	105.9(4)

Table 12
Selected bond distances (Å) and angles (deg) for $Bi_{14}CrO_{24}$ in space group $C2/m$ at 4 K

Cr–O7	1.68(2)	O7–Cr–O8	105(1)	Bi3–O1	2.119(4)	O1–Bi3–O3	92.7(2)
Cr–O8	1.75(1)	O7–Cr–O9	109(1)	Bi3–O3	2.056(5)	O1–Bi3–O4	95.7(2)
Cr–O9	1.61(1)	O7–Cr–O10	112(1)	Bi3–O4	2.246(6)	O1–Bi3–O6	81.9(2)
Cr–O10	1.64(1)	O8–Cr–O9	108.1(6)	Bi3–O6	2.507(6)	O3–Bi3–O4	95.7(2)
		O8–Cr–O10	112.7(7)			O3–Bi3–O6	78.4(2)
		O9–Cr–O10	115.6(7)			O4–Bi3–O6	173.4(2)
				Bi4–O2	2.125(4)	O2–Bi4–O3	95.6(2)
				Bi4–O3	2.229(6)	O2–Bi4–O4	93.3(2)
Bi1–O5	2.279(5)[× 2]	O5–Bi1–O5	71.1(3)	Bi4–O4	2.066(6)	O2–Bi4–O5	82.0(2)
Bi1–O6	2.198(6)[× 2]	O5–Bi1–O6	114.7(3)	Bi4–O5	2.515(6)	O3–Bi4–O4	94.5(2)
		O6–Bi1–O6	74.6(3)			O3–Bi4–O5	173.1(2)
Bi2–O5	2.198(6)[× 2]	O5–Bi2–O5	74.2(3)			O4–Bi4–O5	79.2(2)
Bi2–O6	2.296(5)[× 2]	O5–Bi2–O6	113.9(2)	Bi5–O5	2.354(6)[× 2]	O5–Bi5–O5	106.4(3)
		O6–Bi2–O6	70.9(3)	Bi5–O6	2.359(6)[× 2]	O5–Bi5–O6	69.0(2)
						O6–Bi5–O6	106.9(3)

lone pair of electrons), and Bi2 forms BiO_4e trigonal bipyramids with an equatorial lone pair, as previously reported for the sulfate analogue $Bi_{14}SO_{24}$ (7). In the monoclinic structure, no major changes in the Bi coordination are observed. For the trigonal bipyramids (shown as solid polyhedra in Fig. 11), Bi3–O1, Bi3–O3,

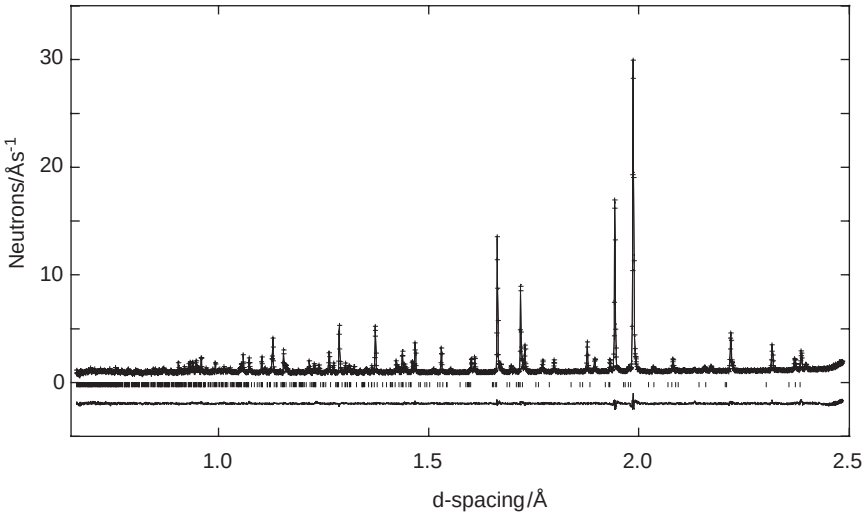

Fig. 9. Observed (+) calculated, and difference NPD profiles for the tetragonal phase of $Bi_{14}CrO_{24}$. Vertical lines mark the reflection positions.

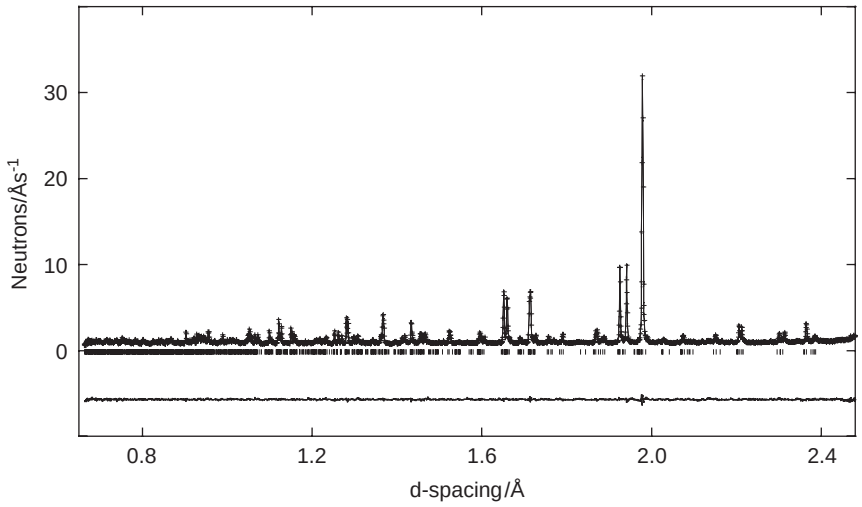

Fig. 10. Observed (+) calculated, and difference NPD profiles for the monoclinic phase of $Bi_{14}CrO_{24}$. Vertical lines mark the reflection positions.

Bi4–O2, and Bi4–O4, are the equatorial bonds whereas Bi3–O4, Bi3–O6, Bi4–O3, and Bi4–O5, are the axial bonds. Tables 10–12 indicate that these Bi–O bond lengths are similar to those reported for $Bi_{14}SO_{24}$. The equatorial and axial bond lengths and O–Bi–O bond angles are also similar to those in α-Bi_2O_3 (12) and β-Bi_2O_3 [13], which contain similar BiO_4e trigonal bipyramids. In all cases the Bi–O equatorial bonds are approximately 2.1 Å and are shorter than the axial bonds: 2.25–2.57 Å for Bi3, and 2.22–2.57 Å for Bi4, for the three monoclinic structures in this study; 2.2–2.3 Å and 2.5–2.6 Å for the two Bi^{3+} ions in α-Bi_2O_3 [12]; 2.3 and 2.5 Å in β-Bi_2O_3 [13]; 2.21 and 2.50 Å for Bi2 in $Bi_{14}SO_{24}$ [7]. The equatorial and axial bond O–Bi3–O angles (92.6–93°/173.4–174.5°), and O–Bi4–O angles (92.8–93.4°/173.1–174.1°), for the three monoclinic structures, are also similar to those in α-Bi_2O_3 (93°/159° and 78°/170°) [12], β-Bi_2O_3 (82°/172°) [13], and O–Bi2–O angles in the tetragonal phases: 78.1°/173° for $Bi_{14}SO_{24}$ [7], 92.8°/174.1° for $Bi_{14}WO_{24}$, 93.2°/174.4° for $Bi_{14}MoO_{24}$ and 93.0°/173.8° for $Bi_{14}CrO_{24}$. The lengthening of the axial bonds and the reduction of the equatorial angle below its ideal value of 120° can be attributable to electron repulsion effects associated with the lone pair of electrons on the Bi^{3+} ions.

The monoclinic distortion has only a small affect on the square pyramidal O atom configurations around Bi1, Bi2 and Bi5. The Bi–O bond distances for the three monoclinic structures (Tables 10–12) are similar to the equivalent bond distances of the tetragonal variants (Tables 4–6) and those for $Bi_{14}SO_{24}$: Bi1–O (2.24 and 2.31 Å), Bi3–O (2.33 Å) [7].

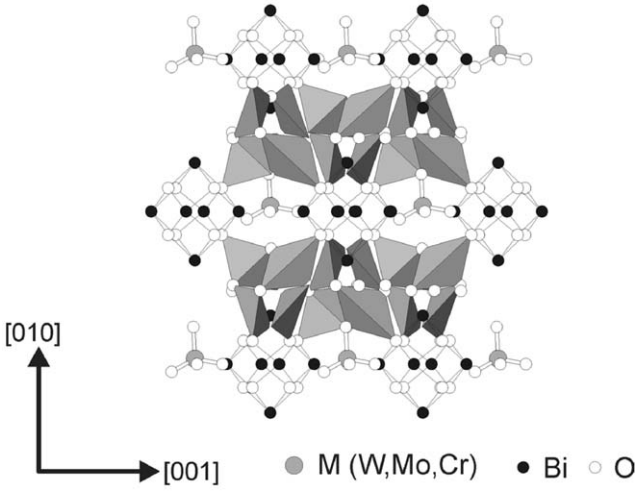

Fig. 11. Structure of the monoclinic phase of $Bi_{14}MO_{24}$ projected along [101]. The solid polyhedra represent BiO_4e trigonal bipyramids. The Bi–O bonds of the BiO_4e square pyramids are marked, as are the M–O bonds of the oxoanions indicating one orientation of the MO_4 group.

4. Conclusions

The results of this investigation have shown that within the temperature range investigated, two distinct phases of $Bi_{14}WO_{24}$, $Bi_{14}MoO_{24}$, and $Bi_{14}CrO_{24}$ occur: a high temperature, body-centered tetragonal phase and a low temperature monoclinic phase. Whereas quenching produced metastable, tetragonal samples of $Bi_{14}WO_{24}$ and $Bi_{14}MoO_{24}$, slow cooling provided the monoclinic polymorph. The structure of the new monoclinic phase has been refined for $Bi_{14}WO_{24}$, $Bi_{14}MoO_{24}$, and $Bi_{14}CrO_{24}$ using TOF, NPD data. The phase change involves no major reorientation of the tetrahedral MO_4 groups, but rotational disorder around the c-axis of the tetragonal phase is reduced, as the 4-fold axis becomes a 2-fold axis in the monoclinic phase.

Acknowledgments

We thank EPSRC for financial support and for the provision of neutron diffraction facilities. We are grateful to K.S. Knight for experimental assistance with the collection of NPD data.

References

[1] T. Takahashi, H. Iwahara, Mater. Res. Bull. 13 (1978) 1447.
[2] H.G. Harwig, A.G. Gerards, Thermochim. Acta 28 (1979) 21.
[3] L.G. Sillén, Ark. Kemi. Mineral. Geol. 12A (1937) 1.
[4] H.A. Harwig, Z. Anorg. Chem. 444 (1978) 151.
[5] S.F. Radaev, V.I. Simonov, Y.F. Kargin, Acta Cryallogr. B 48 (1992) 604.
[6] G. Gattow, H.Z. Schröder, Z. Anorg. Allg. Chem. 318 (1962) 176.
[7] M.G. Francesconi, A.L. Kirbyshire, C. Greaves, Chem. Mater. 10 (1998) 626.
[8] C.D. Ling, R.L. Withers, J.G. Thompson, S. Schmid, Acta Crystallogr. B 55 (1999) 306.
[9] S.A. Warda, W. Pietzuch, W. Massa, U. Kesper, D. Reinen, J. Solid State Sci. 149 (2000) 209.
[10] R.B. Von Dreele, A.C. Larson, M. Lujan, GSAS (1995) Neutron Scattering Center, Los Alamos National Laboratory, Los Alamos, NM 87545.
[11] I.D. Brown, D. Allermatt, Acta Crystallogr. B 41 (1985) 244.
[12] B. Aurivillius, G.K. Malmros, Tekn. Hőgsk. Handl. 291 (1972) 544.
[13] S.K. Blower, C. Greaves, Acta Crystallogr. C 44 (1988) 587.